

# Population study for $\gamma$ -ray pulsars with the outer gap model

J. Takata<sup>1</sup>, Y.Wang<sup>2</sup> and K.S. Cheng<sup>3</sup>

Department of Physics, University of Hong Kong, Pokfulam Road, Hong Kong

Received \_\_\_\_\_; accepted \_\_\_\_\_

---

<sup>1</sup>takata@hku.hk

<sup>2</sup>yuwang@hku.hk

<sup>3</sup>hrspksc@hkucc.hku.hk

## ABSTRACT

Inspired by increase of population of  $\gamma$ -ray emitting pulsars by the *Fermi* telescope, we perform a population study for  $\gamma$ -ray emitting canonical pulsars. We use a Monte-Carlo technique to simulate the Galactic population of neutron stars and the radio pulsars. For each simulated neutron star, we consider the  $\gamma$ -ray emission from the outer gap accelerator in the magnetosphere. In our outer gap model, we apply the gap closure mechanism proposed by Takata et al., in which both photon-photon pair-creation and magnetic pair-creation processes are considered. Simulating the sensitivities of previous major radio surveys, our simulation predicts that there are  $\sim 18 - 23$  radio loud and  $\sim 26 - 34$   $\gamma$ -ray-selected  $\gamma$ -ray pulsars, which can be detected with a  $\gamma$ -ray flux  $F_\gamma \geq 10^{-10}$  erg/cm<sup>2</sup>s. Applying the sensitivity of the six-month observation of the *Fermi* telescope, 40-61 radio-selected and 36-75  $\gamma$ -ray selected pulsars are detected within our simulation. We show that the distributions of various pulsar parameters for the simulated  $\gamma$ -ray pulsars can be consistent with the observed distribution of the  $\gamma$ -ray pulsars detected by the *Fermi* telescope. We also predict that  $\sim 64$  radio-loud and  $\sim 340$   $\gamma$ -ray-selected pulsars irradiate the Earth with a flux  $F_\gamma \geq 10^{-11}$  erg/cm<sup>2</sup>s, and most of those  $\gamma$ -ray pulsars are distributing with a distance more than 1 kpc and a flux  $F_\gamma \sim 10^{-11}$  erg/cm<sup>2</sup>s. The ration between the radio-selected and  $\gamma$ -ray-selected pulsars depend on the sensitivity of the radio surveys. We also discuss the Galactic distribution of the unidentified *Fermi* sources and the canonical  $\gamma$ -ray pulsars.

*Subject headings:* pulsars:general-gamma rays:theory-radiation mechanisms:non-thermal-stars:neutron

## 1. Introduction

The *Fermi*  $\gamma$ -ray telescope has drastically increased population of  $\gamma$ -ray emitting pulsars after its launch in June, 2008. Abdo et al. (2010a) reported the first *Fermi* pulsar catalog, including 21 radio selected pulsars, 16  $\gamma$ -ray-selected pulsars, the Geminga and 8 millisecond pulsars (see also Abdo et al. 2009a,b), while the pulsed radio emissions are reported from several  $\gamma$ -ray-selected pulsars (Camilo et al. 2009). Saz Parkinson et al. (2010) have also reported new eight gamma-ray pulsars discovered in blind searches of *Fermi*-LAT data. These *Fermi* observations for the  $\gamma$ -ray emitting pulsars have started to break the bottleneck of study of the high-energy radiation from the pulsar magnetosphere.

The particle acceleration and resultant high-energy emissions from the pulsar magnetosphere have been studied with polar cap model (Ruderman & Sutherland 1975; Daugherty & Harding 1982, 1996), slot gap model (Arons 1983; Muslimov & Harding 2003; Harding et al. 2008) and outer gap model (Cheng, Ho & Ruderman 1986a,b; Hirotani 2008; Takata, Wang & Cheng 2010; Wang, Takata & Cheng 2010). All emission models assume that the electrons and/or positrons are accelerated by the electric field along the magnetic field lines and that the accelerated particles emit the  $\gamma$ -rays either the curvature radiation or the inverse-Compton processes. The polar cap model assumes the emission region close to the stellar surface and above the polar cap region, while the outer gap and slot gap models assume an acceleration region extending to the outer magnetosphere.

Properties of the pulse profiles and spectra of the  $\gamma$ -ray emission measured by the *Fermi* can be used to discriminate between the different models. For example, most of the observed pulse profiles of the  $\gamma$ -ray pulsars detected by *Fermi* show the double peak structure with a phase-separation of  $\sim 0.4 - 0.5$ , indicating a high-altitude emission from the outer gap or slot gap region is favored more than the low altitude emission from the polar cap accelerator (Romani & Watter 2010; Venter, Harding & Guillemot

2009). Furthermore, in the first *Fermi* pulsar catalog (Abdo et al. 2010a), the spectral fits have been done assuming exponential cut-off function. It is found that the observed spectrum for the Vela pulsar (Abdo et al. 2009c, 2010b) is well fitted by a power law plus hyper-exponential cutoff spectral model of the form  $dN/dE \propto E^{-a} \exp[-(E/E_c)^b]$  with  $b \leq 1$  and  $E_c \sim 1.5$  GeV. This implies that an emission process in the outer magnetosphere is favored more than that near the stellar surface, which predicts a super exponential cut-off ( $b > 1$ ) due to the magnetic pair-creation processes of the  $\gamma$ -rays. In addition, the detection of the radiation above 25 GeV bands associated with the Crab pulsar by the MAGIC telescope has also implied the emission process in the outer magnetosphere (Aliu et al. 2008).

The increase of population of the  $\gamma$ -ray emitting pulsars also allow us to perform a more detail study for the high-energy emissions from the pulsars. Wang et al. (2010) fit the observed phase-averaged spectra using a two-layer outer gap model, and then investigated the relation between the  $\gamma$ -ray luminosity ( $L_\gamma$ ) and the spin down power ( $L_{sd}$ ) for 39  $\gamma$ -ray emitting pulsars including 8 millisecond pulsars. They suggested that the relation can be expressed as  $L_\gamma \propto L_{sd}^\beta$  with  $\beta \sim 0$  for  $L_{sd} \gtrsim 10^{36}$  erg/s, while  $\beta \sim 0.5$  for  $L_{sd} \lesssim 10^{36}$  erg/s. They further argued that the relation between the  $\gamma$ -ray luminosity and the spin-down power implies that the outer gap is closed by the photon-photon pair-creation process for  $L_{sd} \gtrsim 10^{36}$  erg/s (Zhang & Cheng 1997), while by magnetic pair-creation process for  $L_{sd} \lesssim 10^{36}$  erg/s (Takata et al. 2010).

For the outer gap model, the population studies were done to compare the model prediction with the results of *EGRET* instrument (Cheng & Zhang 1998; Zhang et al. 2004; Cheng et al. 2004). Applying the photon-photon pair-creation model for gap closure process, they found that the distributions of the various pulsar parameters (e.g. rotation period, spin down age) were consistent with the observations. Gonthier et al. (2002) and Story, Gonthier and Harding (2007) studied the population of  $\gamma$ -ray pulsars with the polar

cap and slot gap accelerator models to predict the results using the *Fermi* observations. Furthermore, Grenier & Harding (2010) has studied the distribution of the  $\gamma$ -ray pulsars predicted by the outer gap model of Zhang et al. (2004) and for the slot gap model of Muslimov & Harding (2003; 2004) to compare with the *Fermi* results. They have argued that both outer gap and slot gap model may not explain all features of the *Fermi* pulsars; for example, both models predict too few young pulsars compared with the *Fermi* pulsars.

In this paper, we will further develop the population study for the  $\gamma$ -ray emitting pulsars to compare with the results of six-month *Fermi* observations. In particular, we will consider the  $\gamma$ -ray emissions of the canonical  $\gamma$ -ray pulsars with the outer gap model. We will apply the gap closure model proposed by Takata et al. (2010), in which the photon-photon pair-creation process and the magnetic pair-creation process are taken into account. As usual, we will perform a Monte-Carlo simulation for the Galactic population of the neutron star (section 2). In section 2.5, we will discuss our  $\gamma$ -ray emission model and the thickness of the outer gap with the pair-creation processes. In section 3, we will compare the simulated number of the  $\gamma$ -ray pulsars detected on the Earth and its distributions with the *Fermi* observations (section 3.1 and 3.2), and we will predict the future observations (section 3.3). In section 4, we will also discuss ratio of the  $\gamma$ -ray-selected and radio-selected  $\gamma$ -ray pulsars with different radio surveys (section 4.1), and will compare Galactic distributions of the simulated  $\gamma$ -ray pulsars and of the *Fermi* unidentified sources (section 4.2). In section 5, we will summarize the results of our population study.

## 2. Theoretical model and Monte Carlo Simulation

In this section, we will describe our Monte Carlo simulation and  $\gamma$ -ray emission model for the canonical pulsars. First we perform the Monte Carlo simulation for the Galactic neutron stars and for the radio emissions from the pulsars, which have been developed by

several authors (e.g. Sturmer & Dermer 1996; Cheng & Zhang 1998, Gonthier et al. 2002). With this simulation, we will be able to obtain a simulated population of the radio pulsars consistent with the observations. Then we will consider the  $\gamma$ -ray emissions from the outer gap accelerator of each simulated neutron star.

We note that we will sample and discuss the  $\gamma$ -ray emissions from the simulated neutron stars with a characteristic age younger ( $\tau \equiv P/2\dot{P}$ ) than 10 Myr. This is because the present known  $\gamma$ -ray emitting canonical pulsars have their characteristic spin down age less than 5 Myr. Also, we will find that the present  $\gamma$ -ray emission model and the simulation predict that the canonical pulsars with age older than 10 Myr are hard to produce the observable  $\gamma$ -ray emissions in their magnetosphere.

## 2.1. Period and magnetic field

We assume that the neutron stars are born at a rate of 1~2 per century. The initial period of the new born neutron star is not well predicted by theory and observation, except for several cases. For the Crab pulsar, the initial period is estimated at  $P_0 \sim 19$  ms. Such short birth rotation period is also expected by the existence of young 16 ms pulsar PSR J0537-06910 (Marshall et al. 1998). Although most of the new pulsars may have initial period  $P_0 \sim 20$  ms, there is good evidence that some pulsars were born with a longer initial period (e.g.  $P_0 \sim 62$  ms of PSR J1811-1925, Kaspi et. al., 2001). However, we found that the distribution of initial rotation period does not affect much to the following results of the simulation (e.g. the distribution of the radio pulsars and of  $\gamma$ -ray pulsars). For example, we compared the results of two simulations with different distribution of the initial period; one is that all simulated pulsars are randomly distributed in the range  $P_0 = 20 - 30$  ms, and other is that 70 % of pulsars are distributed at  $P_0 = 20 - 30$  ms and 30 % are  $P_0 = 20 - 100$  ms. As we will describe in later, because the pulsars younger than 5 My can

become the  $\gamma$ -ray emitting pulsars, we will sample the pulsars younger than 10 My. For the population of the relatively younger pulsars, we could see that the populations of two simulations are very similar to each other. The difference becomes significant if we assume  $> 50\%$  are randomly distributed in  $P_0 = 20 - 100$  ms. In this paper, therefore, because we do not know well exact distribution of initial rotation period, we randomly choose the initial period in the narrow range  $P_0 = 20 - 30$  ms, such like the assumption in the previous Monte-Carlo studies.

We assume a Gaussian distribution in  $\log_{10} B_s$  for the initial strength of the magnetic field on the stellar surface,

$$\rho_B(\log_{10} B_s) = \frac{1}{\sqrt{2\pi}\sigma_B} \exp \left[ -\frac{1}{2} \left( \frac{\log_{10} B_s - \log_{10} B_0}{\sigma_B} \right)^2 \right], \quad (1)$$

In this study we apply  $\log_{10} B_0 = 12.6$  and  $\sigma_B = 0.1$ , which produce a consistent distribution of the magnetic field of the known radio pulsars derived from the dipole radiation model (Manchester et al. 2005). Because we simulate the neutron stars with a spin down age younger than  $\tau \leq 10$  Myrs, we do not consider the evolution of the magnetic field of each simulated neutron star. The evolution of the stellar magnetic field may be important for the neutron star with an age larger than  $\tau \geq 10$  Myrs (Goldreich & Reisenegger 1992; Hoyos, Reisenegger & Valdivia 2008).

With a constant stellar magnetic field with time, the period evolves as

$$P(t) = \left( P_0^2 + \frac{16\pi^2 R_s^6 B^2}{3Ic^3} t \right)^{1/2}, \quad (2)$$

where we assume the pure dipole radiation,  $R_s$  is the stellar radius and  $I$  is the neutron star momentum of inertia. We apply  $R_s = 10^6$  cm and  $I = 10^{45}$  g  $\cdot$  cm<sup>2</sup> in this study. The time derivative of the rotation period is calculated from

$$\dot{P}(t) = \frac{8\pi^2 R_s^6 B^2}{3Ic^3 P}. \quad (3)$$

## 2.2. Initial spatial and velocity distributions

Following the studies done by Paczynski (1990) and Sturmer & Dermer (1996), we assume the birth location of the neutron star is described by the following distributions,

$$\begin{aligned}\rho_R(R) &= \frac{a_R e^{-R/R_{\text{exp}}} R}{R_{\text{exp}}^2}, \\ \rho_z(z) &= \frac{1}{z_{\text{exp}}} e^{-|z|/z_{\text{exp}}},\end{aligned}\tag{4}$$

where  $R$  is the axial distance from the axis through the Galactic center perpendicular to the Galactic disk and  $z$  is the distance from the Galactic disk. In addition,  $a_R = 20$  kpc,  $R_{\text{exp}} = 4.5$  kpc,  $a_R = [1 - e^{-R_{\text{max}}/R_{\text{exp}}}(1 + R_{\text{max}}/R_{\text{exp}})]^{-1}$  with  $R_{\text{max}} = 20$  kpc and  $z_{\text{exp}} = 75$  pc.

For the distribution of the initial velocity of simulated neutron star, we refer the result of the study for the radio pulsars done by Hobbs et al. (2005). They found that the distribution of the three-dimensional velocity of their sample is well described by a Maxwellian distribution with a characteristic width of  $\sigma_v = 265$  km/s, namely,

$$\rho_v(v) = \sqrt{\frac{\pi}{2}} \frac{v^2}{\sigma_v^3} e^{-v^2/2\sigma_v^2}.\tag{5}$$

We apply this form for the distribution of the initial kick velocity due to the super nova explosion. In this study, we randomly choose the direction of this kick velocity of the neutron star in the three-dimensional space. For the azimuthal component of the velocity, we add the circular velocity due to the Galactic gravitational potential field at the birth position of the neutron star. The circular velocity due to the Galactic potential is calculated from

$$v_{\text{circ}} = \left[ R \left( \frac{\partial \Phi_{\text{sph}}}{\partial R} + \frac{\partial \Phi_{\text{dis}}}{\partial R} + \frac{\partial \Phi_h}{\partial R} \right) \right]^{1/2},\tag{6}$$

where  $\Phi_{\text{sph}}$ ,  $\Phi_{\text{dis}}$  and  $\Phi_h$  are spheroidal, disk and halo components of the Galactic



gravitational potential, which are given by Pacynski (1990) as

$$\Phi_i(R, z) = -\frac{GM_i}{\sqrt{R^2 + [a_i + (z^2 + b_i^2)^{1/2}]^2}}, \quad (7)$$

where  $a_{sph} = 0$ ,  $b_{sph} = 0.277$  kpc and  $M_{sph} = 1.12 \times 10^{10} M_\odot$  for the spheroidal component,  $a_{dis} = 3.7$  kpc,  $b_{dis} = 0.20$  kpc, and  $M_{dis} = 8.07 \times 10^{10} M_\odot$  for the disk component, and

$$\Phi_h(r) = \frac{GM_c}{r_c} \left[ \frac{1}{2} \ln \left( 1 + \frac{r^2}{r_c^2} \right) + \frac{r_c}{r} \tan^{-1} \left( \frac{r}{r_c} \right) \right], \quad (8)$$

where  $r_c = 6.0$  kpc  $M_c = 5.0 \times 10^{10} M_\odot$  for the halo component.

### 2.3. Equation of motion

To obtain current position of each simulated neutron star, we solve the equation of motion from its birth to the current time. The equation of motion is given by

$$\frac{dR^2}{dt^2} = \frac{v_\phi^2}{R} - \frac{\partial \Phi_{tot}}{\partial R}, \quad (9)$$

$$\frac{dz^2}{dt^2} = -\frac{\partial \Phi_{tot}}{\partial z}, \quad (10)$$

and

$$Rv_\phi = \text{constant}, \quad (11)$$

where  $\Phi_{tot} = \Phi_{sph} + \Phi_{dis} + \Phi_h$ , and  $v_\phi$  is the azimuthal component of the velocity. The Lagrangian in units of energy per unit mass is described by

$$L = \frac{v^2(R, z, \phi)}{2} - \Phi_{tot}(R, z) \quad (12)$$

which is used for maintaining an accuracy of the integration of the trajectory described by equations (9) and (10). We maintain the accuracy of one part per  $10^5$  during the trajectory from its birth to the current time.

## 2.4. Radio emission and detection

Because detail process of the radio emission in the pulsar magnetosphere has not been understood well, we apply an empirical relation among the radio luminosity, the rotation period and the period time derivative (Cheng & Zhang 1998; Gonthier et al. 2002). We assume that the radio luminosity at 400 MHz, which is defined by  $L_{400} \equiv d^2 S_{400}$  with  $d$  being the distance and  $S_{400}$  observed flux, for each simulated neutron star follows the distribution (Narayan & Ostriker 1990)

$$\rho_{L_{400}} = 0.5\lambda^2 e^\lambda, \quad (13)$$

where  $\lambda = 3.6[\log_{10}(L_{400}/\langle L_{400} \rangle) + 1.8]$  with  $\log \langle L_{400} \rangle = 6.64 + \frac{1}{3}\log_{10}(\dot{P}/P^3)$ , and  $L_{400}$  is the luminosity in units of mJy kpc<sup>2</sup>. The radio flux on the Earth is given by  $S_{400} = L_{400}/d^2$ . We scale the simulated 400 MHz luminosity to the observation frequency of each survey using a typical photon index -2.

The radio emissions from the pulsars may not point toward the Earth. We apply the radio beaming fraction described as (Emmering & Chevalier 1989)

$$f_r(\omega) = (1 - \cos\omega) + (\pi/2 - \omega) + \sin\omega, \quad (14)$$

where  $\omega$  is the half-angle (in radian) of the radio emission cone and  $0 \leq f_r \leq 1$ . We apply the half-angle of the radio emission cone studied by Kijak & Gil (1998, 2003),

$$\omega_{KG} \sim 0.02 r_{KG}^{1/2} P^{-1/2}, \quad (15)$$

where

$$r_{KG} = 40 \nu_{GHz}^{-0.26} \dot{P}_{-15}^{0.07} P^{0.3},$$

where  $\dot{P}_{-15}$  is the period time derivative in units of  $10^{-15}$  and  $\nu_{GHz}$  is the radio frequency in units of GHz. In the Monte-Carlo simulation, the fraction  $f_r$  of the pulsars with same width  $\omega$  can emit the radio beam toward the Earth.

The minimum detectable radio flux (that is, sensitivity) of a particular radio survey is usually express as (Edwards et al. 2001),

$$S_{min} = \frac{C_{thres}[T_{rec} + T_{sky}(l, b)]}{G\sqrt{2B_{BD}t_i}} \sqrt{\frac{W}{P - W}}, \quad (16)$$

where  $C_{thres}$  is the receiver detection threshold S/N,  $T_{rec}$  is the receiver temperature,  $T_{sky}(l, b)$  is the sky temperature with  $l$  being Galactic longitude and  $b$  Galactic latitude,  $G$  is the telescope gain,  $B_{BD}$  is the band width,  $t_i$  is the integration time and  $W$  is the observed pulse width. The sky temperature at the frequency  $\nu$  is given by (Johnston et al. 1992)

$$T_{sky}(\nu) = 25 + \left\{ \frac{275}{[1 + (l/42)^2][1 + (b/3)^2]} \right\} \left( \frac{408 \text{ MHz}}{\nu} \right)^{2/6} \text{ K}. \quad (17)$$

The observed pulse width is given by

$$W^2 = W_0^2 + \tau_{samp}^2 + \tau_{DM}^2 + \tau_{scat}^2, \quad (18)$$

where  $W_0 \sim 0.05P$  is the intrinsic pulse width,  $\tau_{samp}$  is the receiver sampling time,  $\tau_{DM}$  is the frequency dispersion of the radio pulse as it passes the interstellar medium, and  $\tau_{scat}$  is the frequency dispersion due to the interstellar scattering. The dispersion  $\tau_{DM}$  has the form

$$\tau_{DM} = 8.3 \times 10^6 \text{ DM} \left( \frac{\delta\nu}{\text{MHz}} \right) \left( \frac{\nu}{\text{MHz}} \right)^{-3} \text{ ms} \quad (19)$$

where  $\delta\nu$  is the frequency channel bandwidth of the receiver and DM (in units of  $\text{pc cm}^{-3}$ ) is the dispersion measure, which is calculated from  $\text{DM} = \int n_e(R, Z) ds$ , where  $s$  is the distance to the source and  $n_e(R, Z)$  is electron number density. The Galactic distribution of the electron number density is calculated from the model investigated by Cordes & Lazio (2002). The dispersion due to the interstellar scattering is obtained by

$$\tau_{scat}(\nu) = \tau_{scat,400} \left( \frac{400 \text{ MHz}}{\nu} \right)^{4.4} \text{ ms} \quad (20)$$

where  $\tau_{scat,400} = 10^{-4.61+1.14\log_{10} \text{ DM}} + 10^{-9.22+4.46\log_{10} \text{ DM}}$ .

In Table 1, we list the radio surveys that we applied in the present simulation and its receiver parameters in equations (16)-(20). Also, Figure 1 plots the sensitivity described by equation (16) for each pulsar survey as a function of the period. In Figure 1, we used the sky temperature of  $T_{sky} = 150$  K at 408 MHz and the dispersion measure of  $DM=200$   $\text{cm}^{-3}\text{pc}$ . We note that although new radio pulsars have been reported with the search of the pulsed emissions for the specific sources (e.g. Camilo et al 2009 for *Fermi* sources), the majority of the present radio pulsars have been discovered by the surveys listed in Table 1. Therefore we do not take into account such pulse search for the individual sources.

## 2.5. $\gamma$ -ray emission model

In this section, we describe our  $\gamma$ -ray emission model applied for each simulated pulsar. We consider the  $\gamma$ -ray emission from the outer gap accelerator (Cheng, Ho & Ruderman 1986a,b; Zhang & Cheng 1997; Takata et al. 2010). In the outer gap, the charged particles (electrons and positrons) are accelerated up to a Lorentz factor of  $\Gamma \geq 10^7$  by the electric field along the magnetic field line. The accelerated particles can emit several GeV  $\gamma$ -ray photons through the curvature radiation process. Assuming the force balance between the electric force and the radiation drag force, the Lorentz factor is described by

$$\Gamma = \left( \frac{3R_c^2}{2e} E_{\parallel} \right)^{1/4}, \quad (21)$$

where  $R_c$  is the curvature radius of the magnetic field lines and  $E_{\parallel}$  is the accelerating electric field. The accelerating electric field in the outer gap is approximately described by (Cheng et al. 1986a,b; Cheng, Ruderman & Zhang 2000)

$$E_{\parallel}(r) \sim \frac{B(r)f_{gap}(r)^2 R_{lc}}{R_c}, \quad (22)$$

where  $R_{lc} = cP/2\pi$  is the light radius and  $f_{gap}(r)$  is so called fractional gap thickness in the poloidal plane. The power of the curvature radiation emitted by the individual particle is

written as

$$P_c(E_\gamma, r) = \frac{\sqrt{3}e^2\Gamma}{hR_c}F(x), \quad (23)$$

where  $x = E_\gamma/E_c$  with  $E_c = 3hc\Gamma^3/4\pi R_c$  and

$$F(x) = x \int_x^\infty K_{5/3}(t)dt,$$

where  $K_{5/3}$  is the modified Bessel function of the order 5/3. If the  $\gamma$ -ray beam points toward an observer, the observer will measure the phase-averaged spectrum of (Hirovani 2008),

$$\frac{dF_\gamma}{dE_\gamma} \sim N(r_\xi)R_c(r_\xi)P_c(E_\gamma, r_\xi)\frac{\delta A}{d^2}, \quad (24)$$

where  $N$  is the typical particle number density,  $r_\xi$  represents the typical radius at emission positions from which the emissions can be measured by the observer and  $d$  is the distance to the source. In addition,  $\delta A$  is the cross section of the gap perpendicular to the magnetic field lines and is estimated from  $\delta A \sim [B_s/B(r_\xi)]R_p^2\delta\theta\delta\phi$ , where  $R_p$  is the polar cap radius, and  $\delta\theta$  and  $\delta\phi$  is gap width in the colatitude and azimuthal directions measured on the stellar surface, respectively. For the typical case of the outer gap model, we apply the Goldreich-Julian value,  $N = B/Pce$ , for the number density, and the curvature radius of  $R_c = R_{lc}/2$ . We assume that the outer gap is typically extending to the azimuthal direction with  $\delta\phi \sim \pi$ . The integrated energy flux between 100 MeV and 300GeV can be calculated from

$$F_{\gamma, >100 \text{ MeV}} = \int_{100 \text{ MeV}}^{300 \text{ GeV}} \frac{dF_\gamma}{dE_\gamma} dE_\gamma. \quad (25)$$

In the paper, we assume that the gap current is order of Goldreich-Julian value over the full width as zeroth order approximation. The detailed calculation of the outer gap model (e.g. Takata & Chang 2007) shows that the pair-creation process produces the distribution of the current density in the direction perpendicular to the magnetic field lines. On the other hand, recent two-layer outer gap model (Wang et al. 2010) predicts that total current in the gap is order of the Goldreich-Julian value. Therefore we expect that as long as we

discuss the total power of the  $\gamma$ -ray radiation from the outer gap accelerator, the uniform current distribution with the Goldreich-Julian value would not be bad approximation. The distribution of the current in the gap will be more important to discuss the spectral shape above 100 MeV bands.

The beaming fraction  $f_\gamma$ , which is defined by ratio of the solid angle of the  $\gamma$ -ray beam to  $4\pi$ , affects number of the detected  $\gamma$ -ray pulsars. However, it is complicated to describe the beaming fraction with a simple function. This is because the beaming fraction should be different for different inclination angle and for different pulsars. For the outer gap model, however, the most of emissions concentrate within the direction  $90^\circ \pm 35^\circ$  measured from the rotation axis, as we can see in the photon mappings (e.g. Cheng, Ruderman & Zhang 2000; Takata & Chang 2007), indicating the beaming fraction is roughly  $f_\gamma \sim 35^\circ/90^\circ \sim 0.4$ .

Let's discuss the fractional gap thickness  $f_{gap}$ , which determines the  $\gamma$ -ray flux of equation (24). Recently, Wang et al. (2010) studied the relation between the  $\gamma$ -ray luminosity and the spin down luminosity for the  $\gamma$ -ray pulsars detected by the *Fermi* telescope. They found that the  $\gamma$ -ray luminosity can be described by

$$L_\gamma \propto L_{sd}^\beta \begin{cases} \beta \sim 0, & \text{for } L_{sd} \gtrsim 10^{36} \text{ erg/s} \\ \beta \sim 0.5, & \text{for } L_{sd} \lesssim 10^{36} \text{ erg/s.} \end{cases} \quad (26)$$

They further argued that because the typical  $\gamma$ -ray luminosity is described by  $L_\gamma \sim f_{gap}^3 L_{sd}$ , the change of the relation between  $L_\gamma$  and  $L_{sd}$  indicates the gap closure mechanism in the poloidal plane switches at  $L_{sd} \sim 10^{36}$  erg/s.

The relation that  $L_\gamma \propto L_{sd}^\beta$  with  $\beta \sim 0$  in equation (26) may be understood with the gap closure mechanism proposed by Zhang & Cheng (1997). They argued that the photon-photon pair-creation process between the  $\gamma$ -rays emitted in the outer gap and the X-rays from the stellar surface controls the gap activities. They discussed that the X-rays from the heated polar cap by the return particles will collide with  $\gamma$ -rays in the outer gap

and provide a self-consistent mechanism to restrict the fractional size of the gap. They estimated the typical gap size near the light cylinder as

$$f_{ZC} = 5.5P^{26/21}B_{12}^{-4/7}, \quad (27)$$

where  $B_{12}$  is the polar magnetic field strength in units of  $10^{12}$  G. With this model, the  $\gamma$ -ray luminosity and the spin down power is related as

$$L_{\gamma} \sim 1.3 \times 10^{34} B_{12}^{1/7} L_{sd,36}^{1/14} \text{ erg/s}, \quad (28)$$

where we used  $L_{sd,36}$  is the spin down power in units of  $10^{36}$  erg/s.

On the other hand, the relation that  $L_{\gamma} \propto L_{sd}^{\beta}$  with  $\beta \sim 0.5$  in equation (26) may be explained by the gap closure model proposed by Takata et al. (2010), in which the outer gap is closed by the magnetic pair-creation process near the stellar surface. They argued that the returning particles, which were produced by the photon-photon pair-creation process in the gap, will emit the photons with an energy  $m_e c^2 / \alpha_f \sim 100 \text{ MeV}$  by the curvature radiation near the stellar surface. They discussed that those 100 MeV photons can become pairs by magnetic pair creation process and that these secondary pairs can continue to radiate several MeV photons via the synchrotron radiation. The photon multiplicity is easily over  $10^5$  per each incoming particle. For a simple dipole field structure, all pairs should move inward and cannot affect to the outer gap accelerator. However they argued that the existence of strong surface local field (e.g. Ruderman 1991, Arons 1993) has been widely suggested. In particular if the field lines near the surface, instead of nearly perpendicular to the surface, are bending sideward due to the strong local field, the pairs created in these local magnetic field lines can have an angle bigger than  $90^\circ$ , which results in an outgoing flow of pairs. In fact it only needs a very tiny fraction (1-10) out of  $10^5$  photons creating pairs in these field lines, which are sufficient to provide screening in the outer gap when they migrate to the outer magnetosphere. With this model, they estimated

the fractional gap thickness when this situation occurs as

$$f_m = 0.8KP^{1/2}, \quad (29)$$

where  $K \sim B_{m,12}^{-2}s_7$  is the parameter characterizing the local parameters,  $B_{m,12}$  and  $s_7$  are the local magnetic field in units of  $10^{12}\text{G}$  and the local curvature radius in units of  $10^7\text{cm}$ , respectively. They argued that  $K \sim 2$  for the canonical pulsars, while  $K \sim 15$  for the millisecond pulsars. This gap closure model predicts that the  $\gamma$ -ray luminosity is related with the spin down power as

$$L_\gamma \sim 1.1 \times 10^{34} K^3 B_{12}^{3/4} L_{sd,36}^{5/8} \text{ erg/s}. \quad (30)$$

We can see that the fractional gap thickness  $f_{ZC}$  is smaller than  $f_m$  for the younger pulsar, implying the gap thickness is determined by the photon-photon pair-creation process, while  $f_m < f_{zc}$  for the older pulsars, implying the magnetic pair-creation process may control the gap thickness. Equating  $f_{ZC}$  and  $f_m$ , we obtain the critical spin down power that

$$L_{sd,c} \sim 10^{36} K^{-168/31} B_{12}^{-34/31} \text{ erg/s}, \quad (31)$$

which may explain the switching positions in equation (26) argued by Wang et al. (2010). In this paper, we will investigate the population predicted by the  $\gamma$ -ray emission model with the switching of the gap closure mechanism at  $L_{sd,c}$ , because the population with the emission model without the switching (that is  $f_{gap} = f_{zc}$ ) have been investigated in the previous studies (e.g. Chang and Zhang 1998; Zhang, Zhang and Cheng 2000; Zhang et al. 2004).

Finally we would like to discuss the maximum fractional thickness,  $f_{max}$ , for the active outer gap accelerator. Zhang & Chang (1997) argued that the pulsar with the fractional gap thickness larger than unity,  $f_{ZC} > 1$ , is not active, because the pairs are not created in the gap by the photon-photon pair-creation process. However, it may be possible that the



maximum gap thickness is smaller than unity. For example, outer gap accelerator can exist between the last-open field lines and the critical field lines, on which the Goldreich-Julian charge density is equal to zero at the light cylinder. Therefore, we may define the maximum gap thickness as

$$f_{crit} = \frac{\theta_P - \theta_c}{\theta_p}, \quad (32)$$

where  $\theta_p$  and  $\theta_c$  are polar angles of the last-closed field line and of the critical field line on the stellar surface, respectively. For the pure dipole field, we obtain

$$\theta_p = \alpha + \sin^{-1} \left[ \sin(\theta_{lc} - \alpha) \left( \frac{R_s}{R_{lc}} \sin \theta_{lc} \right)^{1/2} \right] \quad (33)$$

and

$$\theta_c = \alpha + \sin^{-1} \left[ \sin(\theta_n - \alpha) \left( \frac{R_s}{R_{lc}} \sin \theta_n \right)^{1/2} \right], \quad (34)$$

respectively, where  $\alpha$  is the inclination angle,

$$\theta_{lc} = \tan^{-1} \left( \frac{-3 - \sqrt{9 + 8 \tan^2 \alpha}}{4 \tan \alpha} \right),$$

and

$$\theta_n = \tan^{-1} \left( \frac{3 \tan \alpha + \sqrt{8 + 9 \tan^2 \alpha}}{2} \right).$$

In the realistic situation, we expect that the polar cap shape and the magnetic field configuration in the pulsar magnetosphere are more complicated and the simple dipole formulae for  $\theta_p$  and  $\theta_c$  may not be applied. In this paper, therefore, we examine two extreme cases that  $f_{max}=1$  and  $f_{max} = (\theta_p - \theta_c)/\theta_p$  with the dipole field, where we randomly choose the inclination angle  $\alpha$ . These results of the two case may give a range of uncertainty of the present theoretical predictions.

### 3. Results

In this paper, we sample the pulsars with a characteristic age smaller than  $\tau \leq 10$  Myr, because (1) we are interesting in the population study for the  $\gamma$ -ray emitting canonical

pulsars and (2) the present canonical  $\gamma$ -ray pulsars have been detected with a characteristic age younger than 5 Myr. In fact, although we run the simulation to obtain more than 200 times of the present radio pulsars, we could not find any detectable canonical  $\gamma$ -ray pulsars with a characteristic age older than 10 Myr.

We simulate  $3 \times 10^6$  of neutron stars with a constant birth rate during 10 Myrs, and detect 16602 neutron stars as the radio pulsars with a characteristic age of  $\tau \leq 5$ Myr. Scaling the simulated population to the observation,  $\sim 800$  radio pulsars, provides  $\sim 1.3$  per century as the predicted birth rate. Figure 2 compares the distributions of the various characteristics of the simulated (unshaded histograms) and observed pulsars (shaded histograms) with a characteristic age of  $\tau \leq 5$  Myr. We can see in Figure 2 that the present simulation reproduces well the observed distributions for the period time derivative, the spin down age and the surface magnetic field, although the simulation predicts more pulsars close to the Earth and more pulsars with a smaller radio flux, as bottom two panels show. The difference between the results of the observation and of the simulation may be caused by the assumptions within the present simulation. On the other hand, we expect that an adjustment of the slight difference between the simulated and observed population in Figure 2 will not change much the results of population on the  $\gamma$ -ray pulsars discussed in the following sections.

### 3.1. Population “bright” $\gamma$ -ray pulsars

First, we sample only bright  $\gamma$ -ray pulsars, because the  $\gamma$ -ray pulsars with a larger flux measured on the Earth will be preferentially discovered by the *Fermi*  $\gamma$ -ray telescope. Moreover, because the detection of the bright point sources might not be affected much by  $\gamma$ -ray background emissions, it might be true that most of (or all) bright  $\gamma$ -ray pulsars have already discovered by the *Fermi*, implying the distribution of the bright  $\gamma$ -ray sources will

be able to used to test the emission model. In this paper, we define “bright”  $\gamma$ -ray pulsars with a flux larger than  $F_\gamma \geq 10^{-10}$  erg/cm<sup>2</sup>s. In the first *Fermi* pulsar catalog (Abdo et al. 2010a), the number of the bright  $\gamma$ -ray pulsars is 12 for the radio selected and 13 for the  $\gamma$ -ray-selected pulsars (including the Gemniga pulsar). Later, Saz Parkinson et al. (2010) reported new eight  $\gamma$ -ray pulsars discovered in blind frequency searches. Four out of eight pulsars show the  $\gamma$ -ray emissions brighter than  $F_\gamma \geq 10^{-10}$  erg/cm<sup>2</sup>s.

In Table 2, we show the simulated population of the radio-selected  $N_{r,F>10^{-10}}$  and  $\gamma$ -ray-selected  $N_{g,F>10^{-10}}$  bright  $\gamma$ -ray pulsars. We assumed the beaming factor of the  $\gamma$ -ray emissions are  $f_\gamma = 0.4$  and the birthrate is 1.3 per century. We present the results for  $K = 1$  in equation (29), the maximum gap thickness of  $f_{max} = f_{crit}$  and of  $f_{max} = 1$ .

As Table 2 shows, we predict that there are  $N_{r,F>10^{-10}} = 18 \sim 23$  radio-selected and  $N_{g,F>10^{-10}} = 26 \sim 34$   $\gamma$ -ray-selected bright  $\gamma$ -ray pulsars. Although the ratio of the simulated  $\gamma$ -ray-selected to radio-selected bright sources, 1.3-1.5, is consistent with the present *Fermi* bright pulsars, 17/12  $\sim$  1.4, our simulation predicts more number than the observed number (12 radio-selected and 17  $\gamma$ -ray selected pulsars). To explain this difference, we may expect that although all bright sources are actually discovered by the *Fermi*, the detection of the pulsations were failed due to the technical problem, which may be caused by the strong background etc. The recent *Fermi* first source catalog (Abdo et al. 2010c<sup>1</sup>) includes about 50 unidentified sources with a flux  $F_\gamma \geq 10^{-10}$  erg/cm<sup>2</sup>s, and most of them can be categorized as a steady source. The present model indicates that 15  $\sim$  28 of the unidentified *Fermi* bright sources originate from the canonical  $\gamma$ -ray pulsars.

Figure 3 compares cumulative distributions of various characteristics for the simulated and observed bright  $\gamma$ -ray pulsars, including the radio-selected and  $\gamma$ -ray-selected  $\gamma$ -ray

---

<sup>1</sup>[http://fermi.gsfc.nasa.gov/ssc/data/access/lat/1yr\\_catalog](http://fermi.gsfc.nasa.gov/ssc/data/access/lat/1yr_catalog)

pulsars. The results of the simulation are for  $f_{max} = f_{crit}$ . We discuss the combined cumulative distribution of the radio-selected and  $\gamma$ -ray-selected pulsars, (1) because we increase the number of observation sample (12+17=29) to increase the statistical accuracy, and (2) because some  $\gamma$ -ray-selected pulsars have been identified in radio bands (Camilo et al. 2009).

We performed a Kolmogorov-Smirnov (KS) test to compare the two cumulative distributions for the bright sources. In Figure 3, we present the maximum deviation ( $D_{max}$ ) between the two distributions and the p-value ( $P_{ks}$ ) of the KS-test. It can be seen that the hypothesis that the two distributions are drawn from the same parent population can not be rejected at better than  $\sim 80$  % confidence level for the period, spin-down age and the surface magnetic field, than  $\sim 50$  % for the period time derivative and the flux, and than  $\sim 20$  % for the distance, indicating those model distributions will be consistent with the observations.

### 3.2. Comparison with *Fermi* $\gamma$ -ray pulsars

In this section, we present simulated population of the  $\gamma$ -ray pulsars applying the *Fermi* sensitivities of the six-month observations, and compare the simulated population with all known canonical  $\gamma$ -ray pulsars listed in Abdo et al. (2010a) and Saz Parkinson et al. (2010). For the radio-selected  $\gamma$ -ray pulsars, the Fermi sensitivities of the six-month observation is approximately described by  $F = 2 \times 10^{-8}$  photons/cm<sup>2</sup>s for the Galactic latitude  $|b| \geq 5^\circ$  and  $6 \times 10^{-8}$  photons/cm<sup>2</sup>s for  $|b| \leq 5^\circ$ , while for the  $\gamma$ -ray-selected pulsars,  $F = 4 \times 10^{-8}$  photons/cm<sup>2</sup>s for  $|b| \geq 5^\circ$  and  $1.2 \times 10^{-7}$  photons/cm<sup>2</sup>s for  $|b| \leq 5^\circ$ .

Figures 4 and 5 show the distributions for the various characteristics for the radio-selected and  $\gamma$ -ray-selected  $\gamma$ -ray pulsars, respectively. The shaded and un-shaded

histogram show the results for the *Fermi* pulsars and simulated pulsars, respectively. The maximum deviation of the cumulative distributions ( $D_{max}$ ) and the p-value of the K-S test ( $P_{ks}$ ) are also indicated in each panel. The results are for  $f_{max} = f_{crit}$ . We can see that except for the distributions of the period time derivative of the radio-selected  $\gamma$ -ray pulsars,  $p$ -value of the K-S test is larger than  $P_{ks} \sim 0.15$ , indicating hypothesis that the two distributions are drawn from the same parent population can not be rejected at better than  $\sim 85\%$ . Therefore, we would conclude that distributions of the our simulation are not conflict with the *Fermi* observations.

Although KS-statistic indicates the consistency between the simulated and the observed distributions, one can see an excess in the observed distribution (shaded histograms in Figures 4 and 5) compared with the simulated distribution at rotation period  $P \sim 0.1$  s, the spin down age  $\tau \sim 10^5$  yr and the distance  $d \sim 1$  kpc. This may be cause by intrinsic feature of the pulsars or selection effect or enhancement of the birth rate due to the local Galactic structure. Because the excess is caused by only three or four pulsars, all possibilities can be considered. If the excess of the pulsars is due to the local structure, the Gould Belt may be possible site to produce the pulsars which make the excess in the distributions. For example, Cheng et al. (2004) discussed that about 20  $\gamma$ -ray pulsars with a flux  $F_\gamma \geq 7 \times 10^{-11}$  are associated with the Gould Belt. The Gould Belt has an ellipsoidal ring with semi-major and semi-minor axes equal to  $\sim 0.5$  and  $0.35$  kpc, respectively (Guillout et al. 1998), although a smaller size is also predicted (c.f. Perrot & Grenier 2002). The distance to the center of the Gould Belt from the Sun is  $\sim 0.1$ kpc, indicating the neutron stars are born about 0.25-0.6 kpc away from the Sun. If we use the typical velocity of the neutron star  $\sim 300$  km/s, the displacement during  $\tau \sim 10^5$  yr is  $d \sim 300$  km/s  $\times 10^5$  yr  $\sim 0.1$ kpc. Such a small displacement will not be able to explain the excess of the distance at 1 kpc, although the size of the Gould Belt can play an important role. We expect that if the excess in the distributions are caused by the selection effects or by the effect of Gould Belt, the excess

will decrease as increase of the  $\gamma$ -ray pulsar population. On the other hand, if it is the intrinsic feature of the pulsar population, the excess will remain even the population of the pulsars increase.

In Table 2, we show the number of the simulated radio-selected ( $N_{rtot}$ ) and  $\gamma$ -ray-selected ( $N_{gtot}$ )  $\gamma$ -ray pulsars. Our simulation predicts that with the present sensitivity, the *Fermi* can detect  $N_{rtot} = 40 - 61$  of the radio-selected  $\gamma$ -ray pulsars and  $N_{gtot} = 36 - 75$  of the  $\gamma$ -ray-selected  $\gamma$ -ray pulsars, which are more than the present *Fermi* pulsars, that is, 21 radio-selected and 24  $\gamma$ -ray selected pulsars (Abdo et al. 2010a; Saz Parkinson et al. 2010). To explain the difference between the observation and the model, the several reasons are expected; because most of the canonical  $\gamma$ -ray pulsars are located in the Galactic disk (c.f. Figure 10), 1) the simulated sensitivity of the *Fermi* is too simple, namely, the sensitivity becomes much worse at the Galactic plane ( $|b| \sim 0$ ), 2) a strong  $\gamma$ -ray background prevents the detection of the pulsed emissions from some pulsars, and (3) the  $\gamma$ -ray emissions from the pulsars may be missed by source confusion with the complex regions (e.g. Cygnus and Carina that lie on tangents to spiral arms), and/or with the unresolved sources that are not modeled in the diffuse backgrounds.

As Table 2 shows, our simulation also predicts that if the *Fermi* sensitivity increase factor of two from the present one, *Fermi* can in principle detect  $N_{rtot \times 2} = 58 - 89$  radio-selected and  $N_{gtot \times 2} = 79 - 152$   $\gamma$ -ray-selected  $\gamma$ -ray pulsars.

### 3.3. Implication for future observations

Finally, we discuss model implication on future observations. In the observation, sensitivity of the detection of  $\gamma$ -ray emitting pulsars really depend on the observed direction (that is, high or Galactic latitude) and  $\gamma$ -ray-selected or radio-selected pulsars, implying the

present observed distribution of the pulsar characteristics may not represent the intrinsic population of the  $\gamma$ -ray pulsars that irradiate the Earth.

Figure 6 summarizes number of the pulsars detected within the simulation as a function of the  $\gamma$ -ray threshold energy flux. Here, because we do not take into account the dependency of the sensitivity on the observed direction and on the radio-selected or  $\gamma$ -ray-selected pulsars, Figure 6 presents the intrinsic number of the pulsars irradiating the Earth with a flux larger than the threshold flux. The solid and dashed lines represent numbers for the radio-selected and  $\gamma$ -ray-selected  $\gamma$ -ray pulsars, respectively. In addition, the thin and thick lines are results for the fractional gap thicknesses of  $f_{max} = f_{crit}$  and  $f_{max} = 1$ , respectively. In the simulation, for example, 18-23 radio-selected (solid lines) and 27-35  $\gamma$ -ray-selected (dashed line)  $\gamma$ -ray pulsars irradiate the Earth with a flux large than  $F_\gamma = 10^{-10}$  erg/cm<sup>2</sup>s measured on the Earth, while 64-89 radio-selected and 340-441  $\gamma$ -ray-selected  $\gamma$ -ray pulsars irradiate the Earth with a flux larger than  $F_\gamma = 10^{-11}$  erg/cm<sup>2</sup>s. Our simulation therefore implies that although the minimum energy flux of the known  $\gamma$ -ray pulsars is approximately  $F_\gamma \sim 10^{-11}$  erg/cm<sup>2</sup>s, the *Fermi* has missed most of the  $\gamma$ -ray pulsar with a  $\gamma$ -ray flux larger than  $F_\gamma = 10^{-11}$  erg/cm<sup>2</sup>s.

Figures 7 and 8 show the distributions (unshaded histograms) of characteristics of the simulated radio-selected and  $\gamma$ -ray-selected  $\gamma$ -ray pulsars, respectively, with a  $\gamma$ -ray flux larger than  $F_\gamma \geq 10^{-11}$  erg/cm<sup>2</sup>s. In the figures we also show the observed distributions (dashed histograms) by the *Fermi*. For the rotation period, the simulation predicts that the future observations will detect the radio-loud pulsars with longer rotation period ( $P > 0.5$  s) as Figure 7 shows, if the sensitivity is improved. For the  $\gamma$ -ray-selected pulsars, on the other hand, the future observations will detect more pulsars with a shorter rotation period than 0.1 s.

We find in Figures 7 and 8 that most of the simulated pulsars distribute with a distance

around  $d \sim 10$  kpc and a flux  $F_\gamma \sim 10^{-11}$  erg/cm<sup>2</sup>s, while the distributions of the *Fermi* pulsars have a peak at  $d \sim 1$  kpc and  $F_\gamma \sim 10^{-10}$  erg/cm<sup>2</sup>s. Therefore, our simulation predicts that as the sensitivity is improved, more and more  $\gamma$ -ray pulsars with a distance larger than  $d \sim 1$  kpc and a flux smaller than  $F_\gamma \sim 10^{-10}$  erg/cm<sup>2</sup>s will be detected by the future observations.

We note that as Figures 7 and 8 show, our simulation indicates the peak of distributions for the period and the period time derivative come to  $P \sim 0.1 - 0.3$  s and  $\dot{P} \times 5 \times 10^{-14}$  s/s, respectively, indicating the  $\gamma$ -ray pulsars with a rotation period of  $P \sim 0.1 \sim 0.3$  s and a period time derivative of  $\dot{P} \sim 5 \times 10^{-14}$  s/s may be preferentially detected from the unidentified Galactic sources. This information might be useful to narrow down the searching range of the pulse period from the unidentified sources to detect new  $\gamma$ -ray-selected pulsars.

## 4. Discussions

### 4.1. Ratio between radio-selected and $\gamma$ -ray-selected pulsars

In this section, we discuss the ratio between the radio-selected and  $\gamma$ -ray-selected  $\gamma$ -ray pulsars. With Table 3, we demonstrate how the ratio depend on the radio surveys. The first column shows the radio surveys used in the simulation, where M2, A2, and P2 represent for Molonglo 2, Arecibo 2 and Parks 2 surveys. “All” presents results with all radio surveys listed in Table 1. In addition, we increase factor of two for the sensitivity of each survey. The second and third column show the number of the radio-selected ( $N_r$ ) and the  $\gamma$ -ray selected pulsars that irradiate the Earth with a flux larger than  $F_\gamma = 10^{-10}$  erg/cm<sup>2</sup>s and  $10^{-11}$  erg/cm<sup>2</sup>s, respectively. The fourth column shows the results using the *Fermi* sensitivity of six-month observations. We present the results for  $f_{max} = f_{crit}$ .



As Table 3 shows the ratio between the radio-selected and radio-quiet  $\gamma$ -ray pulsars depend on the sensitivity of the radio survey. For example, the present simulation predicts the ratio  $N_g/N_r = 4$  using only Arecibo 2 and Parks 2 surveys, which will be consistent with the  $N_g/N_r = 37/11 \sim 3.4$  predicted by Cheng & Zhang (1998). Because radio emissions from some  $\gamma$ -ray selected pulsars can be detected by more sensitive radio survey, the ratio using “All” radio survey listed in Table 1 becomes  $N_g/N_r \sim 1.4$ , which will be consistent with the present *Fermi* result  $N_g/N_r \sim 17/12 \sim 1.4$ .

Table 3 indicates that the ratio depends on the threshold energy flux, that is, the ratio increases as the threshold energy flux decreases, as second and third columns show. This tendency depends on the sensitivity of the radio survey. For example, because the “bright”  $\gamma$ -ray sources are located relatively near the Earth, the radio emissions from those pulsars can be observed by the present radio surveys if the radio emissions point toward the Earth. On the other hand, dimmer  $\gamma$ -ray sources ( $F_\gamma \sim 10^{-11}$  erg/cm<sup>2</sup>s) tend to have a more distance as indicated by bottom panels of Figures 7 and 8. The flux of radio emissions from those distant  $\gamma$ -ray pulsars may be under the sensitivity of the radio surveys, and the pulsars are categorized as  $\gamma$ -ray-selected pulsars. Therefore, the ratio of the  $\gamma$ -ray-selected and radio-selected pulsars increases as the threshold energy flux decreases. In fact, the present simulation predict that if we could detect all pulsars that irradiate the Earth with the radio emissions, the ratio of the  $\gamma$ -ray-selected and radio-selected pulsars does not depend on the threshold energy flux.

Applying the sensitivity of the *Fermi* (fourth column), because the sensitivity for the radio-selected  $\gamma$ -ray pulsars is better than the  $\gamma$ -ray-selected pulsars, the ratio  $N_g/N_r$  is in general smaller than those of second and third columns, whose sensitivities for the radio-selected and  $\gamma$ -ray-selected  $\gamma$ -ray pulsars are the same each other. With the all radio surveys, the ration  $N_r/N_g \sim 0.9$  will be consistent with the six-month *Fermi* observations,

$$N_r/N_g \sim 24/21 \sim 1.1.$$

#### 4.2. Comparison with unidentified *Fermi* sources

Finally, we discuss the distributions of the  $\gamma$ -ray pulsars in the galaxy. As we discussed in section 3.3, the present model predicts most of the canonical  $\gamma$ -ray pulsars with a flux smaller than  $F_\gamma \leq 10^{-10}$  erg/cm<sup>2</sup>s have been missed by the *Fermi* telescope. On the other hand, the *Fermi* has found several hundreds of the unidentified points sources, implying some of them must be the canonical  $\gamma$ -ray pulsars. It will be useful to compare the Galactic distributions for the simulated  $\gamma$ -ray pulsars and the unidentified sources to have a hint for the origin of the unidentified sources. Figures 9 and 10, respectively, show the Galactic longitude and latitude distributions for the simulated  $\gamma$ -ray pulsars with  $F_\gamma \geq 10^{-11}$  erg/cm<sup>2</sup>s (solid line) and the unidentified *Fermi* sources (dashed line). We selected the unidentified sources with the criteria that the observed  $\gamma$ -ray flux is larger than  $10^{-11}$  erg/cm<sup>2</sup>s and the variability index (V) in the catalog smaller than 23.21, larger than which indicates less than a 1% chance of being a steady source (Abdo et al. 2010c). In addition, we chose the unidentified sources with the curvature index, which is defined in the first catalog, larger than 5. A curvature index larger than 11.34 indicates a less than 1 % chance that the power-law spectrum is a good fit for 100 MeV-100GeV. The first catalog show that the  $\gamma$ -ray pulsars typically have a curvature index larger than 5.

We find in Figure 9 that the Galactic longitude distribution of the simulated  $\gamma$ -ray pulsars is qualitatively consistent with that of the *Fermi* unidentified sources, that is, both distributions have a peak around  $l = 0^\circ$  and become minimum around  $l \sim 180^\circ$ . In fact, we can see that the distributions of the existing radio pulsars younger than the characteristic age of  $\tau \leq 5$  Myr is also qualitatively consistent with that of the unidentified sources.

In Figure 10, on the other hand, we can see that most of the simulated  $\gamma$ -ray pulsars are located around the Galactic disk, that is,  $|b| < 5^\circ \sim 10^\circ$ , while significant fraction of the unidentified sources are located above the Galactic disk. Because we could see that the longitudinal distribution of the simulated  $\gamma$ -ray pulsars is consistent with that of the existing radio pulsars younger than the characteristic age  $\tau \leq 5$  Myr, our model prediction is that most of high-latitude unidentified sources will not associate with the canonical  $\gamma$ -ray pulsars. If the majority of the unidentified sources is originated from the Galactic sources, the millisecond pulsars may be possible candidate. Because millisecond pulsars are in general older than the canonical  $\gamma$ -ray pulsars and have a slower proper motion than the canonical pulsars, they are bounded by the Galactic potential. It is expected that a more fraction of  $\gamma$ -ray emitting millisecond pulsars is located at the higher Galactic latitude. On these ground, it will be important to perform a population study of the millisecond  $\gamma$ -ray pulsars to reveal the origin of the *Fermi* unidentified sources. The results of the population study for the millisecond pulsars using a Mont-Carlo technique will be discussed in the subsequent papers.

## 5. Conclusion

Inspired by the drastically increase of the  $\gamma$ -ray emitting pulsars by the *Fermi* telescope, we performed a population study for the canonical  $\gamma$ -ray pulsars with a Monte-Carlo method. We applied the outer gap model with a switching of the gap closure process from the photon-photon pair-creation to the magnetic pair-creation model suggested by Takata et al. (2010). Our simulation predicts that there are 18-23 radio-selected and 26-34  $\gamma$ -ray-selected  $\gamma$ -ray pulsars with a flux larger than  $10^{-10}$  erg/cm<sup>2</sup>s measured on the Earth. Applying *Fermi* sensitivity of six-month observations, our simulation predicts that 40 – 61 radio-selected and 36-75  $\gamma$ -ray-selected pulsars can be detected. We showed that the

simulated distributions for the various characteristics (e.g. rotation period, characteristic age) can successfully explain those of the *Fermi*  $\gamma$ -ray pulsars. Our simulation also predicts that there are  $\sim 64$  radio-selected and  $\sim 340$   $\gamma$ -ray-selected  $\gamma$ -ray pulsars irradiate the Earth with a  $\gamma$ -ray flux larger than  $F_\gamma \geq 10^{-11}$  erg/cm<sup>2</sup>s. This indicates that most of the  $\gamma$ -ray pulsars have been missed by the present observations, although their fluxes are larger than the minimum  $\gamma$ -ray flux detected by the *Fermi* so far. In particular, our simulation predicts that if the sensitivity of the instrument is improved, more  $\gamma$ -ray pulsars located with a distance larger than 1 kpc and a flux  $F_\gamma \sim 10^{-11}$  erg/cm<sup>2</sup>s will be detected by in the future observations. The ratio of the simulated  $\gamma$ -ray-selected to radio-selected  $\gamma$ -ray pulsars is  $\sim 1.4$  for  $F_\gamma \geq 10^{-10}$  erg/cm<sup>2</sup>s, while  $\sim 1$  using 6-month *Fermi* sensitivity, although the ratio depends on the sensitivities of the radio surveys. Finally, we compared the Galactic distributions between the simulated  $\gamma$ -ray pulsars and unidentified *Fermi* sources. We saw that although the Galactic longitude distribution of the simulated  $\gamma$ -ray pulsars is qualitatively consistent with that of the *Fermi* unidentified sources, the simulated latitude distribution can not explain the observations, in particular for the higher latitude sources. This may suggest that the population study for the  $\gamma$ -ray emitting millisecond pulsars may help to understand the origin of the high-latitude *Fermi* unidentified sources.

We thank the useful discussions with H.-K. Chang, K. Hirotani, C.Y. Hui, B. Rudak, M.Ruderman and S.Shibata. We express our appreciation to the anonymous referee for useful comments, which led to a much improved manuscript. We also thank to Theoretical Institute for Advanced Research in Astrophysics (TIARA) operated under Academia Sinica Institute of Astronomy and Astrophysics, Taiwan, which enables author (J.T.) to use PC cluster at TIARA. This work is supported by a GRF grant of Hong Kong SAR Government under HKU700908P.

## REFERENCES

Abdo A.A. et al., 2010a, ApJS, 187, 460

Abdo A.A. et al., 2010b, ApJ, 713, 154

Abdo A.A. et al., 2010c, ApJS, 188, 405

Abdo A.A. et al., 2009a, Sci., 325, 848

Abdo A.A. et al., 2009b, Sci., 325, 840

Abdo A.A. et al., 2009c, ApJ, 696, 1084

Aliu E. et al., 2008, Sci, 322, 1221

Arons J., 1993, ApJ, 408, 160

Arons J., 1983, ApJ, 266, 215

Camilo F. et al. 2009, ApJ, 705, 1

Cheng, K.S., Zhang, L., Leung, P. & Jiang, Z.J., 2004, ApJ, 608, 418

Cheng K.S., Ruderman M. & Zhang L. 2000, ApJ, 537, 964

Cheng K.S. & Zhang, L. 1998, ApJ, 498, 327

Cheng K.S., Ho C. & Ruderman M. 1986a, ApJ, 300, 500

Cheng K.S., Ho C. & Ruderman M. 1986b, ApJ, 300, 522

Clifton, T.R., Lyne, A.G., Jones, A.W., McKenna, J.& Ashworth, M., 1992, MNRAS, 254,

177

Cordes, J.M. & Lazio, T.J.W., 2002, preprint (astro-ph/0207156)

- Dewey, R.J., Taylor, J.H., Weisberg, J. M. & Stokes, G.H., 1985, ApJL, 294, 25
- Grenier I.A. & Harding A.K., 2010, 2010, 12-16 April “High Energy Emission from Pulsars and Their Systems”, Sant Cugat, Spain
- Goldreich P. & Reisenegger A. 1992, ApJ, 395, 250
- Gonthier, P.L., Ouellette, M.S., Berrier, J., O’Brien, S, Harding, A.K., 2002, ApJ, 565, 482
- Guillout, P., Sterzik, M.F., Schmitt, J.H.M.M., Motch, C., & Neuhaeuser, R., 1998, A&A, 337, 113
- Daugherty J.K. & Harding, A.K., 1996, ApJ, 458, 278
- Daugherty J.K. & Harding, A.K., 1982, ApJ, 252, 337
- Edwards, R.T., Bailes, M., van Straten, W. & Britton, M.C., 2001, MNRAS, 326, 358
- Emmering, R.T. & Chevalier, R.A., 1989, ApJ, 345, 931
- Gonthier, P.L., Ouellette, M.S., Berrier, J., O’Brien, S, & Harding, A.K., 2002, ApJ, 565, 482
- Harding A.K., Stern J.V., Dyks J. & Frackowiak M., 2008, ApJ, 680, 1378
- Hirota K., 2008, ApJL, 688, 25
- Hobbs, G., Lorimer, D.R., Lyne, A. G. & Kramer, M., 2005, MNRAS, 360, 974
- Hoyos, J., Reisenegger, A. & Valdivia, J. A., 2008, A& A 487, 789
- Johnston, S., Lyne, A.G., Manchester, R.N., Kniffen, D.A., D’Amico, N., Lim, J.& Ashworth, M., 1992, MNRAS, 255, 401

- Kaspi, V.M., Roberts, M.E., Vasisht, G., Gotthelf, E.V., Pivovarov, M. & Kawai, N., 2001, ApJ, 560, 371
- Kijak, J. & Gil, J., 2003, A& A, 397, 969
- Kijak, J. & Gil, J., 1998, MNRAS, 299, 855
- Marshall, F.E., Gotthelf, E.V., Zhang, W., Middleditch, J. & Wang, Q. D., 1998, ApJL, 499, 179
- Manchester, R.N., Hobbs, G.B., Teoh, A. & Hobbs, M., Astron. J., 129, 1993-2006 (2005) (astro-ph/0412641)
- Manchester, R.N. et al., 2001, MNRAS, 328, 17
- Manchester, R.N. et al., 1996, MNRAS, 279, 1235
- Manchester, R.N., Lyne, A.G., Taylor, J.H., Durdin, J.M., Large, M.I. & Little, A.G., 1978, MNRAS, 185, 409
- Muslimov, A.G. & Harding A.K., 2004, ApJ, 617, 471
- Muslimov, A.G. & Harding A.K., 2003, ApJ, 588, 430
- Narayan, R. & Ostriker, J.P., 1990, ApJ, 352, 222
- Nice, D.J., Taylor, J.H. & Fruchter, A.S., 1993, ApJL, 402, 49
- Paczynski, B., 1990, ApJ, 348, 485
- Peroot, C.A., & Grenier I.A., 2003, A&A, 404, 519
- Romani R.W. & Watter K.P., 2010, ApJ, 714, 810
- Ruderman M., 1991, ApJ, 366, 261

- Ruderman M.A. & Sutherland P.G., 1975, ApJ, 196, 51
- Saz Pstkinson, P.M. et al. 2010, arXiv:1006.2134
- Stokes, G.H., Segelstein, D.J., Taylor, J.H. & Dewey, R.J. 1986, ApJ, 311, 694
- Story, S.A., Gonthier, P.L. & Harding, A.K., 2007, ApJ, 671, 713
- Sturmer, S.J. & Dermer, C.D., 1996, A& AS, 120, 99
- Takata J., Wang, Y. & Cheng, K.S., 2010, ApJ, 715, 1318
- Takata J. & Chang H.-K., 2007 ApJ, 670, 677
- Wang, Y., Takata, J., & Cheng, K.S., 2010, ApJ, 720,178
- Venter C., Harding A.K. & Guillemot L., 2009, ApJ, 707, 800
- Zhang L., Cheng K.S., Jiang Z.J. & Leung P., 2004, ApJ, 604, 317
- Zhang L. Zhang, Y. J. & Cheng, K. S., 2000, A& A, 357, 957
- Zhang L. & Cheng K.S., 1997, ApJ, 487, 370



Survey	Gain (KJy <sup>-1</sup> )	$C_{thres}$	$T_{rec}$ (K)	$\nu$ (MHz)	$t_i$ (s)	$\tau_{samp}$ (ms)	$B_{BD}$ (MHz)	$\delta\nu$ (MHz)	$l$ (degree)	$b$ (degree)	References
Molonglo 2	5.1	5.4	210	408	40.96	40	3.2	0.8	[0,360]	[-85,20]	Manchester et al. (1978)
Green Bank 2	0.89	7.5	30	390	137	33.5	16	2	[0,360]	[-18,90]	Dewey et al. (1985)
Green Bank 3	0.95	8	30	390	131	2.2	8	0.25	[0,360]	[-18,90]	Stokes et al. (1986)
Arecibo 2	10.9	8	90	430	39.3	0.4	0.96	0.06	[40,65]	[-10,10]	Stokes et al. (1986)
Arecibo 3	13.35	8.5	75	430	68.2	0.5	10	0.078	[35,65]	[-8,8]	Nice et al. (1993)
Parkes 1	0.24	8	45	1520	157	2.4	320	5	[270,20]	[-4,4]	Johnston et al. (1992)
Parkes 2	0.43	8	50	436	157	0.6	32	0.125	[0,360]	[-90,0]	Manchester et al. (1996)
Parks MB	0.735	24	21	1374	2100	0.250	285	3	[260,50]	[-5,5]	Manchester et al. (2001)
Jordell Bank 2	0.4	6	40	1400	524	4	40	5	[355,105]	[-1,1]	Clifton et al. (1992)
Swinburne IL	0.64	15	21	1374	265	0.125	288	3	[260,50]	[5,15]	Edwards et al. (2001)

Table 1: Parameters of each radio survey.

Number	$N_{r,F>10^{-10}}$	$N_{g,F>10^{-10}}$	$N_{rtot}$	$N_{gtot}$	$N_{rtot \times 2}$	$N_{gtot \times 2}$
K=1 $f_{max} = 1$	23	34	61	75	89	152
$f_{max} = f_{crit}$	18	26	40	36	58	79

Table 2:  $N_{r,F>10^{-10}}$  and  $N_{g,F>10^{-10}}$  are the number of the simulated radio-selected and  $\gamma$ -ray-selected pulsars with a flux of  $F \geq 10^{-10}$  erg/cm<sup>2</sup>s, respectively.  $N_{rtot}$  and  $N_{gtot}$  present number of the simulated radio-selected and  $\gamma$ -ray-selected pulsars using *Fermi* sensitivity of the six-month observations; for the radio-selected pulsars,  $F = 2 \times 10^{-8}$  photons/cm<sup>2</sup>s for the  $|b| \geq 5^\circ$  and  $6 \times 10^{-8}$  photons/cm<sup>2</sup>s for  $|b| \leq 5^\circ$ , while for the  $\gamma$ -ray-selected pulsars,  $F = 4 \times 10^{-8}$  photons/cm<sup>2</sup>s for  $|b| \geq 5^\circ$  and  $1.2 \times 10^{-7}$  photons/cm<sup>2</sup>s for  $|b| \leq 5^\circ$ . For  $N_{rtot \times 2}$  and  $N_{gtot \times 2}$ , we increases factor of two for the *Fermi* sensitivity.

Survey	$N_r$	$N_g$	$N_g/N_r$	$N_r$	$N_g$	$N_g/N_r$	$N_r$	$N_g$	$N_g/N_r$
	$F_\gamma \geq 10^{-10}$ erg/cm <sup>2</sup> s			$F_\gamma \geq 10^{-11}$ erg/cm <sup>2</sup> s			<i>Fermi</i> sensitivity		
A2, P2	9	35	3.9	24	372	15.5	17	48	2.8
M2, A2, P2	13	28	2.2	36	367	10.2	26	40	1.5
All	18	26	1.4	64	340	5.3	40	36	0.9
All ( $\times 2$ )	20	26	1.3	93	319	4.2	47	34	0.72

Table 3: Ratio between the radio-selected ( $N_r$ ) and  $\gamma$ -ray-selected ( $N_g$ ) pulsars vs. radio surveys. The first column is list of survey, the second and the third columns present the number of the pulsars detected within the simulation with  $F_\gamma \geq 10^{-10}$  erg/cm<sup>2</sup>s and  $F_\gamma \geq 10^{-11}$  erg/cm<sup>2</sup>s, respectively. The final column shows the number of the pulsars detected within the simulation using the *Fermi* sensitivity of the six-month observation. The results are for the beaming fraction of  $f_\gamma \sim 0.4$  and the birth rate of 1.3 per century. M2=Molonglo 2, A2=Arecibo 2 and P2=Parks 2. “All” represents all surveys listed in Table 1. In “All( $\times 2$ )”, we increase factor of two for the sensitivity of each survey.

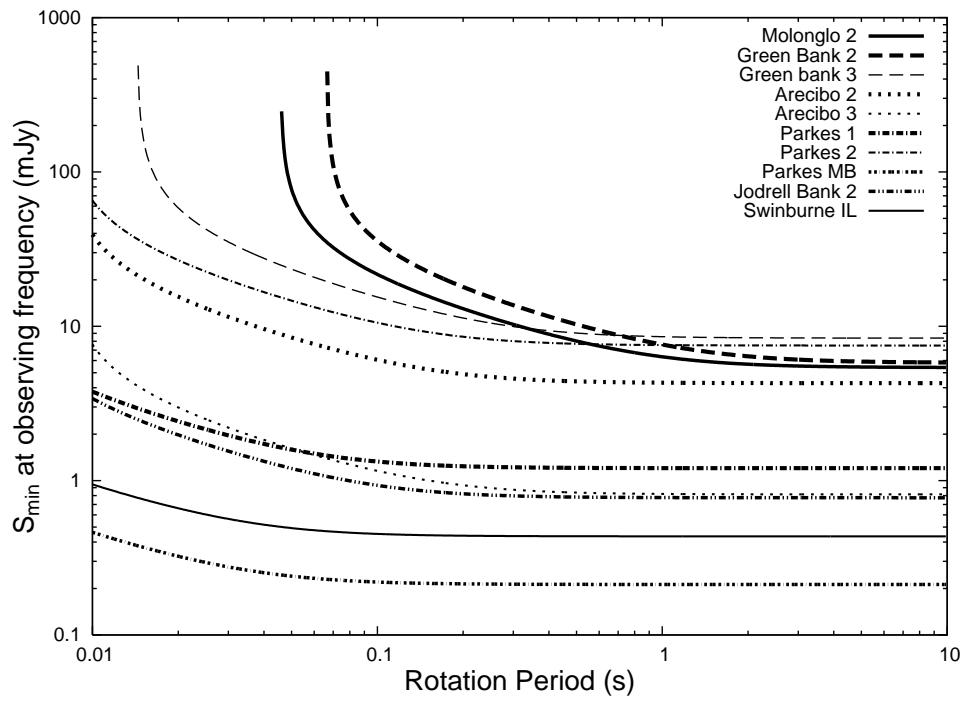


Fig. 1.— Radio flux threshold for each radio survey as a function of the rotation period. The results are for  $T_{sky} = 150$  K at 408 MHz and the dispersion measure of  $DM = 200 \text{ cm}^{-3}\text{pc}$ .

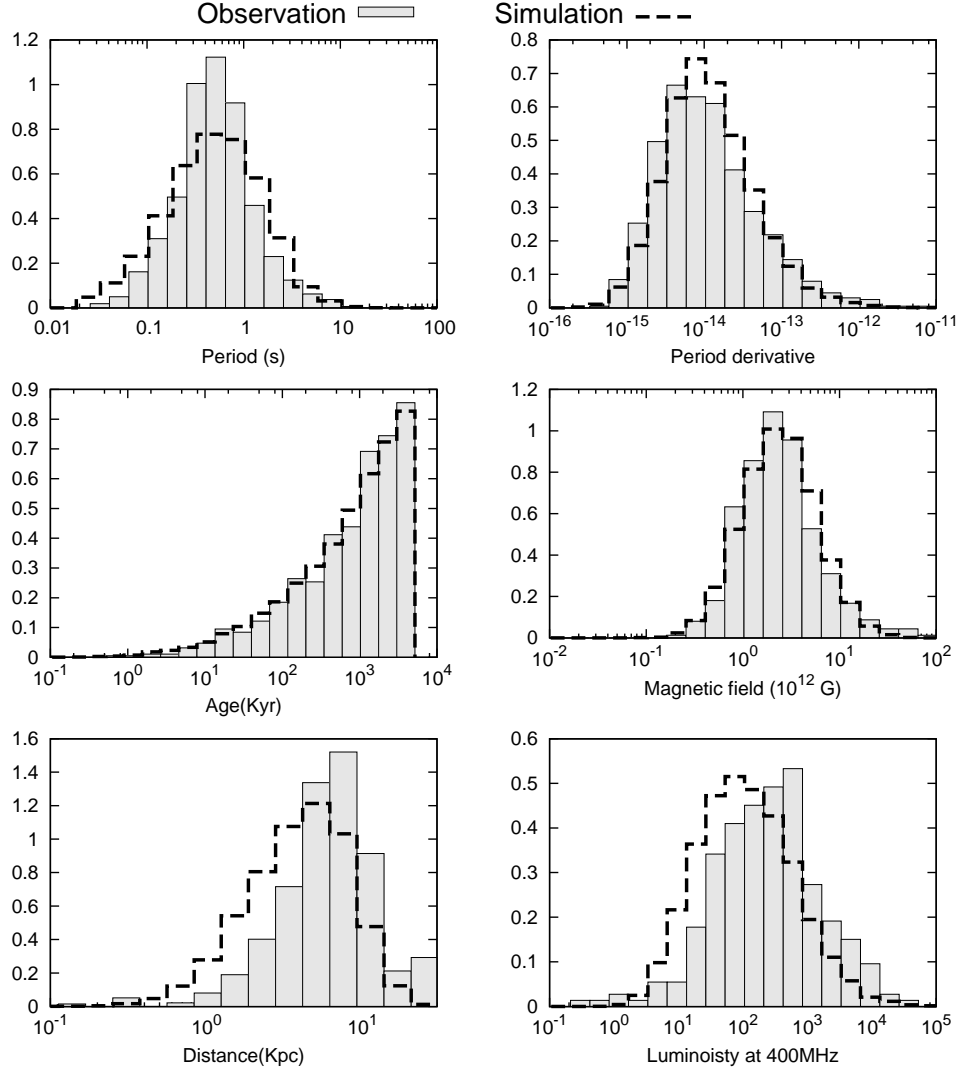


Fig. 2.— Distributions of various characteristics of the radio pulsars with a characteristic age ( $\tau = P/2\dot{P}$ ) younger than 5 Myr. The shaded histograms and unshaded histograms present results for the observation and simulation, respectively. The data were taken from Manchester et al. (2005).

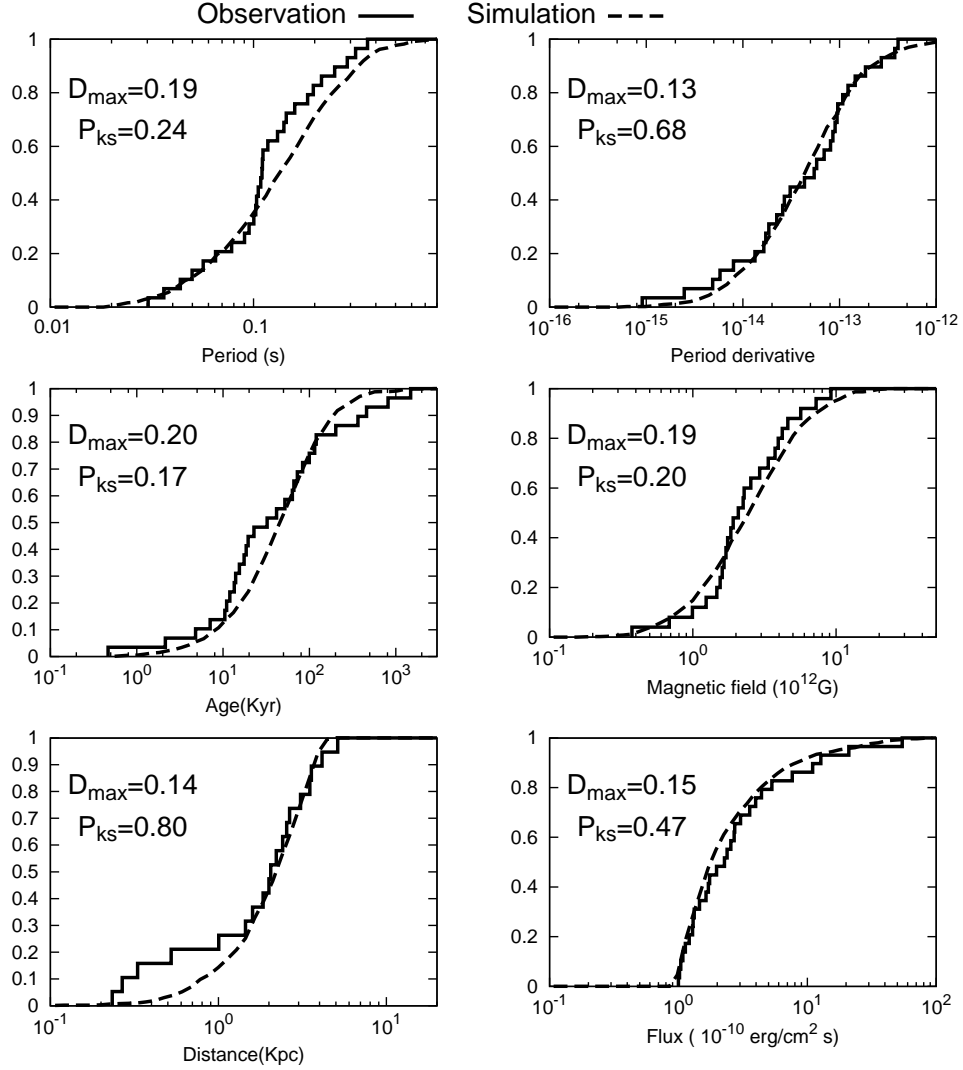


Fig. 3.— Comparison of the cumulative distributions for the various characteristics of “bright”  $\gamma$ -ray pulsars,  $F_{\gamma} \geq 10^{-10}$  erg/cm $^2$ s, including both radio-selected and  $\gamma$ -ray-selected  $\gamma$ -ray pulsars. The solid and dashed lines represent the distributions for the observations and for the simulation, respectively. The p-value ( $P_{KS}$ ) of the Kolmoglov-Smirov test and the maximum difference ( $D_{max}$ ) between two distributions are also indicated in each panel. The data were taken from Abdo et al. (2010a) and Saz Parkinson et al. (2010).

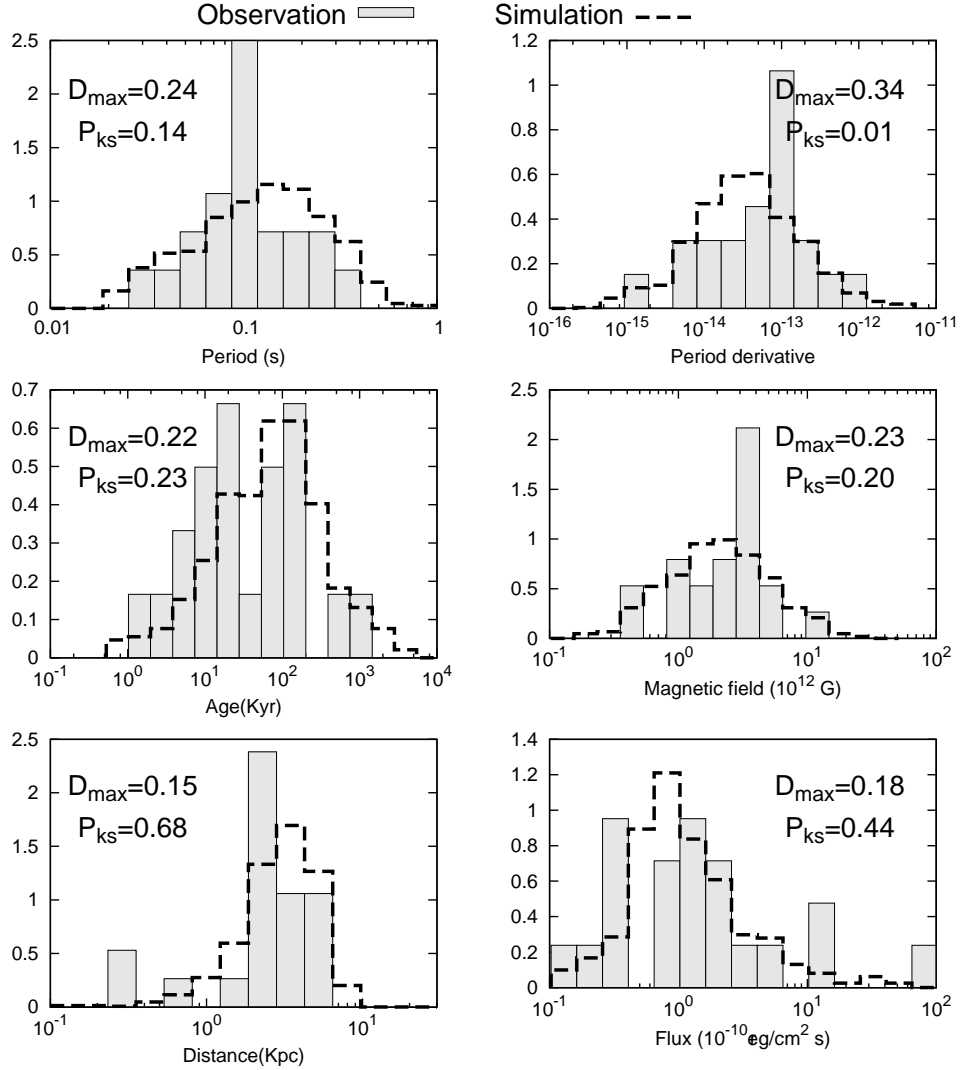


Fig. 4.— The distribution of the various characteristics for the radio-selected  $\gamma$ -ray pulsars for six-month *Fermi* observations. The shaded and unshaded histograms presents results for the observations and for the simulation, respectively. In addition,  $D_{\max}$  and  $P_{\text{KS}}$  show the maximum difference of the cumulative distributions and the p-value of the KS-test, respectively. In the simulation, the sensitivity of the  $\gamma$ -ray detection is set at  $F = 2 \times 10^{-8}$  photons/cm<sup>2</sup>s for  $|b| \geq 5^\circ$  and  $6 \times 10^{-8}$  photons/cm<sup>2</sup>s for  $|b| \leq 5^\circ$ . The data were taken from Abdo et al. (2010a) and Saz Parkinson et al. (2010).

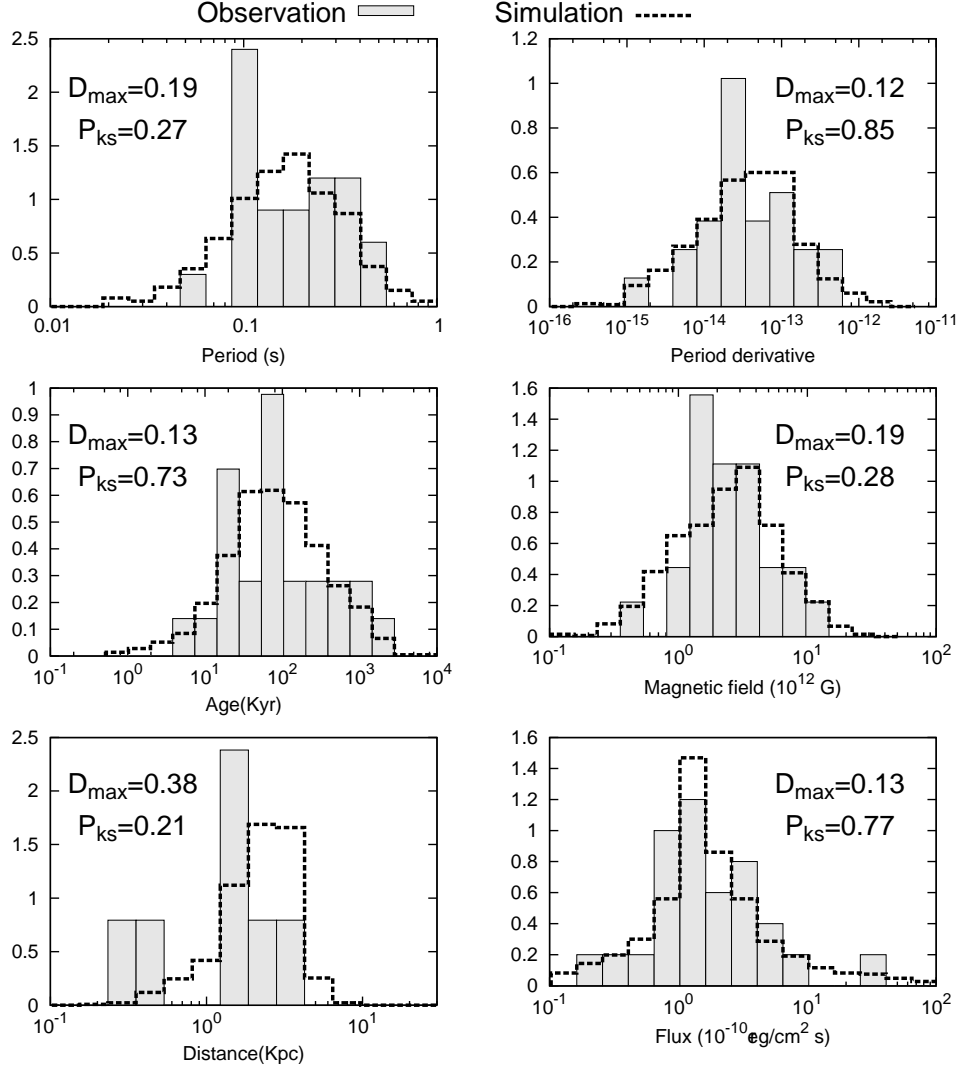


Fig. 5.— The same with Fig. 4, but results for the  $\gamma$ -ray-selected  $\gamma$ -ray pulsars. In the simulation, the sensitivity of the  $\gamma$ -ray detection is set at  $F = 4 \times 10^{-8}$  photons/cm<sup>2</sup>s for  $|b| \geq 5^\circ$  and  $1.2 \times 10^{-7}$  photons/cm<sup>2</sup>s for  $|b| \leq 5^\circ$ .



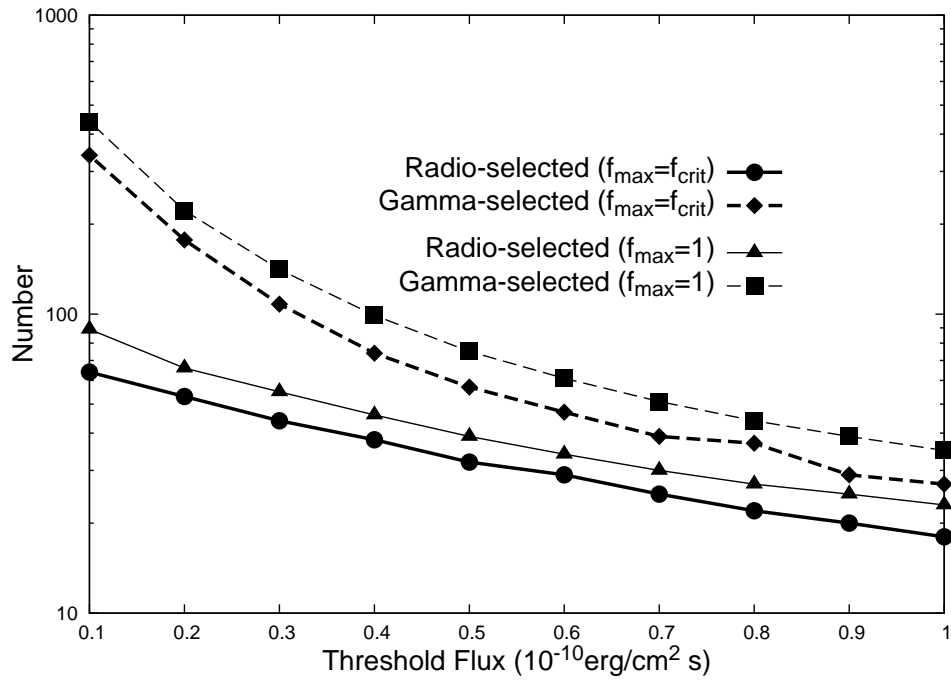


Fig. 6.— The number of radio-selected (solid) and  $\gamma$ -ray-selected (dashed) pulsars detected within simulation as a function of the threshold energy flux. The thick and thin lines are results for the maximum fractional gap thickness of  $f_{\text{max}} = f_{\text{crit}}$  and  $f_{\text{max}} = 1$ , respectively.

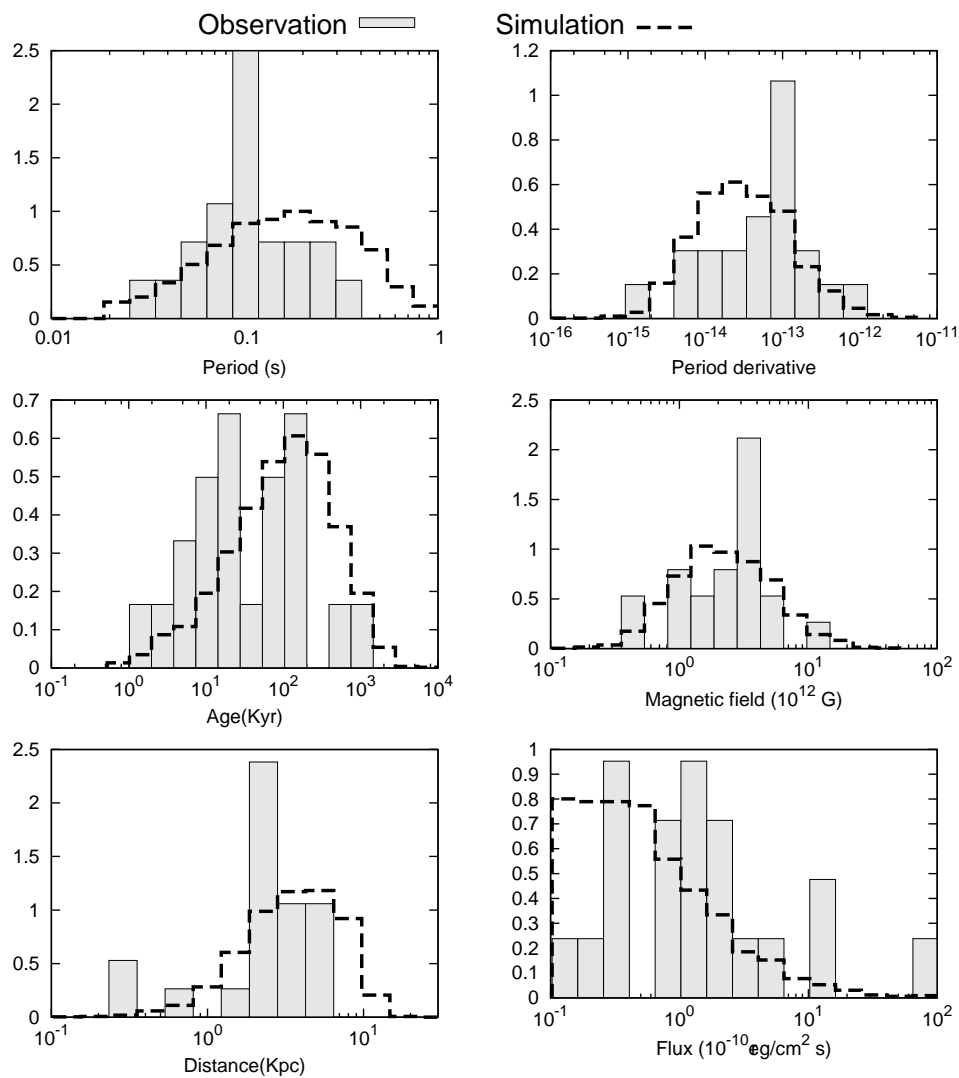


Fig. 7.— The simulated distribution (unshaded histograms) of the characteristics for the radio-selected  $\gamma$ -ray pulsars that irradiate the Earth with a flux  $F_\gamma \geq 10^{-11}$  erg/cm<sup>2</sup>s. The shaded histograms present results for the *Fermi* observation.

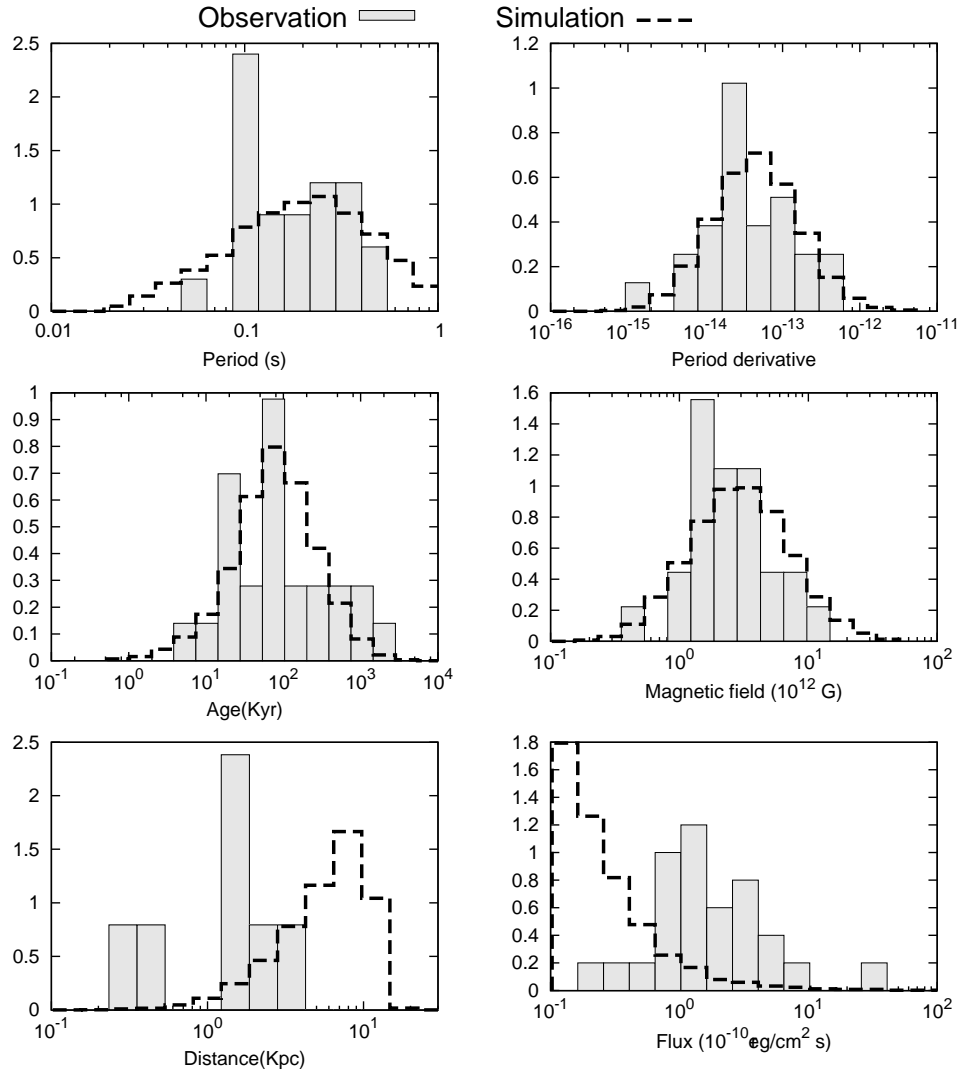


Fig. 8.— The same with Fig. 7, but results for the  $\gamma$ -ray-selected pulsars.

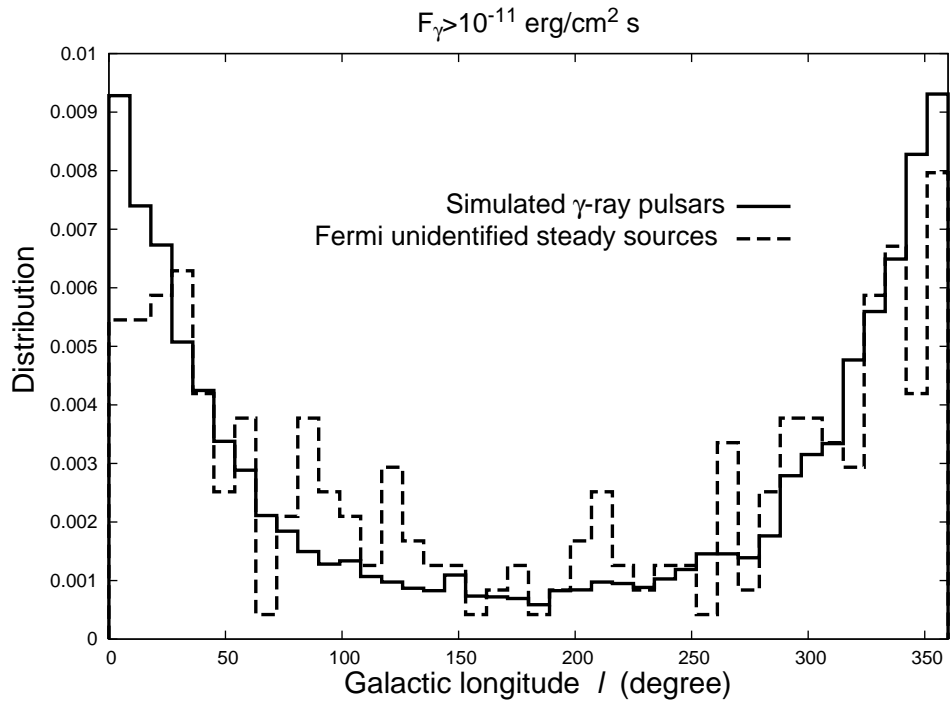


Fig. 9.— The Galactic longitude distributions of the simulated  $\gamma$ -ray pulsars (solid line) and the *Fermi* unidentified sources with  $F_\gamma \geq 10^{-11} \text{ erg/cm}^2 \text{ s}$ . The data were taken from the *Fermi* first catalog (Abdo et al., 2010c) with the criteria that the variable index less than 23.11 and the curvature index larger than 5.

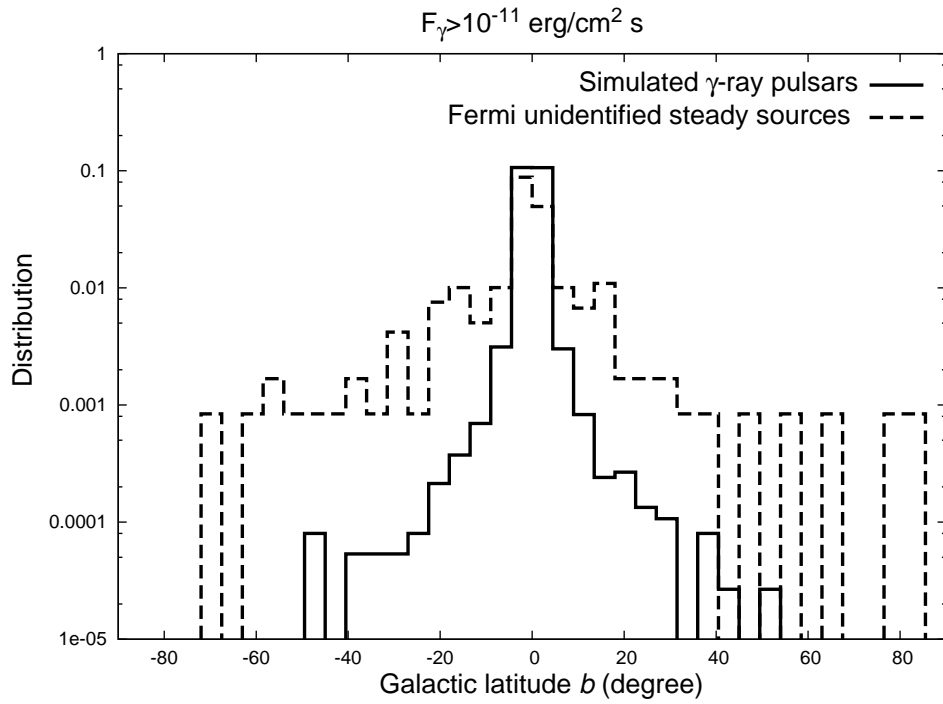


Fig. 10.— The Galactic latitude distributions of the simulated  $\gamma$ -ray pulsars (solid line) and the *Fermi* unidentified sources with  $F_\gamma \geq 10^{-11} \text{ erg/cm}^2 \text{ s}$ . The data were taken from Abdo et al. (2010c).